Growth and Saturation of the Electron Drift Instability in a Crossed Field Plasma

Zachariah A. Brown and Benjamin A. Jorns

Phys. Rev. Lett. **130**, 115101 — Published 13 March 2023

DOI: 10.1103/PhysRevLett.130.115101

Growth and Saturation of the Electron Drift Instability in a Crossed-Field Plasma

Zachariah A. Brown* and Benjamin A. Jorns
University of Michigan
(Dated: January 31, 2023)

The linear growth and nonlinear energy transfer of the electron drift instability (EDI) are experimentally measured in the plume of a low-temperature, Hall effect discharge. A frequency-based bispectral analysis technique applied to fast ion density fluctuation measurements shows a growth rate function that is qualitatively similar to predictions from the linear instability dispersion relation, but an order of magnitude smaller. Calculation of the nonlinear transfer function indicates multiple three-wave interactions between high-frequency resonances of the instability in addition to an inverse energy cascade towards lower-frequency modes. These results are discussed in the context of recent theoretical, numerical, and experimental efforts on the EDI in Hall effect discharges and how the EDI may impact anomalous cross-field transport.

The onset and growth of instabilities is a nearly universal phenomenon in plasma physics [1–4]. Understanding the dynamics of these instabilities is of practical importance as they can drive "anomalous" particle and energy fluxes that dominate the plasma state. This transport can result in undesirable effects such as poor confinement and low efficiency [5]. The electron drift instability (EDI) is a particularly widespread type of transport-inducing wave that is known to impact several space-based and low-temperature plasma devices with crossed electric and magnetic fields [2, 5–7]. This electrostatic mode, which is driven unstable by an $E\times B$ electron drift coupled to electron cyclotron resonances[8–11], has been linked to reduced efficiency in ion sources[12], anomalous heating of particles in the magnetosphere[13], and self-organization in pulsed magnetron sputtering devices[6].

Despite the widespread existence of the EDI, several aspects of this instability remain poorly understood. Foremost among these is the degree to which this instability directly impacts anomalous particle and energy flux. In practice, quantifying these effects requires an understanding of the growth rate—the rate at which the EDI extracts momentum from the background plasma—and the power spectrum—the distribution of energy in the waves as a function of frequency and lengthscale[14]. While there are many theories for these aspects of the EDI[4, 15–19], there has yet to be a direct experimental measurement of the linear growth and nonlinear wave coupling processes that govern the EDI spectrum. This lack of experimental data speaks to a broader problem commonly encountered in measuring wave dynamics in low temperature plasmas [5]: established methods based on length-scale bispectral analysis[20, 21], developed for higher energy density plasmas, do not translate well to space-based and low temperature systems. This stems primarily from limitations in spatial resolution and spectral bandwidth.

In light of these obstacles and the importance of understanding the processes that shape the EDI growth spectra, we motivate in this Letter a frequency-based bispectral analysis technique to make direct experimental measurements of the linear growth and nonlinear energy transfer of the EDI in a laboratory Hall effect discharge. We describe in the following the theory of the method, the experimental technique, and a comparison of the results to linear theory.

Our approach to measuring the EDI dynamics is based on formulating a nonlinear governing wave equation for its evolution. We then use experimental measurements of the wave properties combined with a bispectral analysis method adapted from the works of Ritz [20] and Kim [21] to infer the parameters in the wave equation that represent linear and nonlinear growth. Figure 1 shows the geometry of the Hall effect discharge we investigated with this approach. This device has azimuthal symmetry with an axial electric field and radial magnetic field. The resulting azimuthal $E\times B$ drift is the energy source for driving the EDI unstable. For our analysis, we adopt the local Cartesian coordinate system shown in Fig. 1. Following the eikonal approximation (c.f. [22]), we represent the spectrum of oscillations as a superposition of fluctuations in plasma potential, $\phi(\vec{r},t) = \sum_{\vec{k},\omega}\phi(\vec{k},\omega)$ where we have invoked a two-scale representation of the waves: $\phi(\vec{k},\omega) = \hat{\phi}(\vec{k},\omega)\exp\left[i\left(\vec{k}\cdot\vec{r}-\omega t\right)\right]$. Here the exponential denotes the rapidly oscillating component of the mode in the EDI spectrum with real frequency, ω, and real wavevector, $\vec{k}$, while $\hat{\phi}(\vec{k},\omega)$ is the more slowly evolving complex amplitude of this mode.

To motivate a governing equation for $\phi(\vec{k},\omega)$, we consider the evolution of each propagating mode in space and time. This approach is inspired by Ref. [22] where a governing equation for the complex amplitude of the waves, $\hat{\phi}(\vec{k},\omega)$, is derived from a perturbation analysis of the electrostatic dispersion relation. In a departure from this work, however, we also have included a term that accounts for the evolution of the rapidly oscillating component of the mode, $\exp\left[i\left(\vec{k}\cdot\vec{r}-\omega t\right)\right]$ (c.f. [23]). We thus find

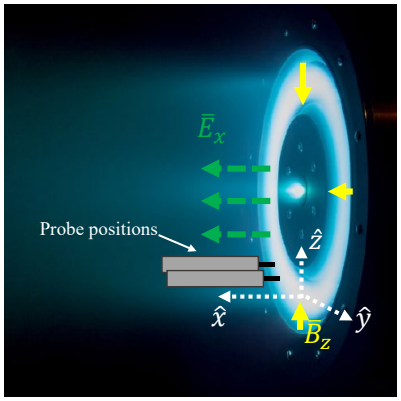

FIG. 1: H9 Hall thruster shown with axial electric field ($\bar{E}$), radial magnetic field ($\bar{B}$), and probes placed in the $E \times B$ direction.

$$\frac{\partial\phi(\vec{k},\omega)}{\partial t} + \vec{v}_g \cdot \frac{\partial\phi(\vec{k},\omega)}{\partial\vec{r}} = \gamma_\omega \phi(\vec{k},\omega) \quad (1)$$
$$+ i\left(\vec{k}\cdot\vec{v}_g - \omega\right)\phi(\vec{k},\omega) + \sum_{\substack{\omega=\omega_1+\omega_2 \\ \vec{k}=\vec{k}_1+\vec{k}_2}} V^Q_{1,2}\phi(\vec{k}_1,\omega_1)\phi(\vec{k}_2,\omega_2).$$

On the left hand side, the first term of Eq. 1 represents the change in time while the second is the convection in space at the group velocity $\vec{v}_g = -\partial_{\vec{k}}\epsilon_r^{(1)}(\vec{k},\omega)/\partial_\omega\epsilon_r^{(1)}(\vec{k},\omega)$. Here $\epsilon^{(1)}(\vec{k},\omega)$ is the dielectric response to first order. On the right hand side, the first term denotes the linear growth of the wave $\gamma_\omega = -\epsilon_i^{(1)}(\vec{k},\omega)/\partial_\omega\epsilon_r^{(1)}(\vec{k},\omega)$. This physically is the rate at which energy is extracted from the background plasma as the mode propagates. It primarily impacts the magnitude of the complex wave amplitude, $\hat{\phi}(\vec{k},\omega)$. We note that this definition for linear growth, which results from an expansion of the dielectric response of the plasma, is contingent on the existence of an imaginary component of the dielectric. While in the case of wave propagation entirely perpendicular to the magnetic field, the dielectric function of the EDI is entirely real [10], the presence of a component parallel to the magnetic field leads to an imaginary component of the dielectric [24]. In turn, we have found for the range of parallel wavenumbers we anticipate for this study, the above definition of linear growth is approximately equal to the imaginary component of the frequency roots of the dispersion. The second term in Eq. 1 stems from the evolution of the rapidly oscillating component of the wave. The third term represents the change in the wave induced from three-wave coupling interactions that satisfy $\vec{k} = \vec{k}_1 \pm \vec{k}_2$ and $\omega = \omega_1 \pm \omega_2$. The coefficient $V^Q_{1,2}$ is a weighting function for the strength of each three-wave interaction and is related to the second order dielectric response[22].

Eq. 1 is a framework for relating change in wave amplitude to linear growth and nonlinear contributions. To translate this result into a form that can be analyzed experimentally, we Fourier transform with respect to time:

$$\vec{v}_g \cdot \frac{\partial\hat{\phi}_f}{\partial\vec{r}} = \left(\gamma_f + i\vec{k}_r\cdot\vec{v}_g\right)\hat{\phi}_f + \sum_{f=f_1+f_2} V^Q_{1,2}\hat{\phi}_{f_1}\hat{\phi}_{f_2}, \quad (2)$$

where we have introduced $\hat{\phi}_f$, the complex amplitude of the Fourier transform with respect to time at frequency, $f = \omega/2\pi$ in the EDI spectrum. We note that in translating Eq. 1 to Eq. 2, we have made the approximation that if there is a set of frequencies f_1, f_2 that satisfies $f_1 \pm f_2 = f$, there is only one set of wavevectors, $\vec{k}_1, \vec{k}_2$, that satisfies $\vec{k}_1 \pm \vec{k}_2 = \vec{k}$. This is consistent with the form of the EDI that applies to our plasma (Fig. 2a) and allows us to simplify the summation in Eq. 2 to frequency combinations.

To arrive at a method for experimentally inferring the growth, we consider Eq. 2 for the configuration shown in Fig. 1 where two electrostatic probes are separated azimuthally by distance, Δy. These probes simultaneously measure the time-based Fourier spectrum at each location to yield $X_f = \hat{\phi}_f(y)$ and $Y_f = \hat{\phi}_f(y+\Delta y)$. Based on these two measurement locations, we can discretize Eq. 2 with respect to the azimuthal coordinate to find

$$Y_f = L_f X_f + \sum_{f=f_1+f_2} Q^{1,2}_f X_{f_1} X_{f_2}, \quad (3)$$

where we have linear and nonlinear transfer functions:

$$L_f = \left[\left(\gamma_{f(y)}/v_{g(y)} + ik_y\right)\Delta y + 1 - i\Delta\Theta_f\right]e^{i\Delta\Theta_f} \quad (4)$$
$$Q^{1,2}_f = e^{i\Delta\Theta_f} V^Q_{1,2}\Delta y/v_{g(y)}.$$

Here $\Delta\Theta_f$ is the phase difference between the two measurement points for oscillations at frequency f and is determined from the cross-power spectrum: $\exp(i\Delta\Theta_f) = Y_f X_f^*/|Y_f X_f^*|$. Additionally, we have introduced the azimuthal linear growth rate, $\gamma_{f(y)} = \gamma_f - \mathrm{Re}\left(X_f^{-1}\left[v_{g(x)}\partial_x X_f + v_{g(z)}\partial_z X_f\right)\right]$. This nomenclature reflects the fact that the formalism only tracks changes in the azimuthal wave properties. This term may differ from the total growth if there are contributions from the orthogonal directions. We return to this point in the discussion. Finally, we multiply Eq. 2 by the complex conjugate quantities, X_f^* and $X_{f_1}^* X_{f_2}^*$ respectively, to yield

$$Y_f X_f^* = L_f X_f X_f^* + \sum_{f=f_1+f_2} Q^{1,2}_f X_{f_1} X_{f_2} X_f^* \quad (5)$$
$$Y_f X_{f_1}^* X_{f_2}^* = L_f X_f X_{f_1}^* X_{f_2}^* + \sum_{f=f_1+f_2} Q^{1,2}_f X_{f_1} X_{f_2} X_{f_1}^* X_{f_2}^*.$$

The first equation is the complex form of a discretized wave energy equation. The second represents the third moment of the wave-dynamics, i.e. the cross-bispectrum.

With experimental measurements of the moments in Eq. 5, e.g. $X_{f_1}X_{f_2}X_f^*$, the system can be solved for the linear, L_f, and nonlinear, $Q_f^{1,2}$, transfer functions. In turn, from these measurements, we can infer the azimuthal growth rate, $\gamma_{f(y)} = (\mathrm{Re}[L_f]-1)(v_{g(y)}/\Delta y)$. We also can use our experimentally-informed estimates of the transfer functions to determine aspects of the nonlinear coupling. Most relevantly, we introduce a governing equation for the wave energy density, $P_f = |\hat{\phi}|^2$, by multiplying Eq. 2 by the complex conjugate. This yields in the azimuthal direction $\partial_y P_f = 2\gamma_f P_f + T_f$ where T_f represents the energy flux transferred to the mode of frequency f by nonlinear coupling from other modes in the spectrum. Following Ref. [20], we can relate this last term to the nonlinear transfer function:

$$T_f = (v_{g(y)}/\Delta y)\mathrm{Re}\left[\sum_{f=f_1+f_2} e^{-i\Delta\Theta_f} Q_f^{1,2} X_{f_1} X_{f_2} X_f^*\right]. \quad (6)$$

We solve our governing equations following the algorithmic approach developed by Ritz [20] and later modified by Kim [21]. While in this previous work, the spatial Fourier transform of Eq. 1 was considered, we have formulated our equations in terms of the time-based Fourier transform. We adopted this approach because it was not possible to insert a sufficient number of probes in our small scale plasma to perform spatial transforms. Despite our use of a frequency based analysis, the form of equations remains the same and thus the same algorithm can be applied. To this end, this analysis method has two key requirements. The first is ensemble averaging the various moments in Eq. 5 over multiple measurements to reduce stochastic noise[25]. The second requirement is that the ensemble averaged power spectra, $P_f = \langle X_f X_f^* \rangle \approx \langle Y_f Y_f^* \rangle$, are stationary between the two probe locations[21]. This assumption is justified by the azimuthal symmetry of the discharge (Fig. 1).

As a last step before we can leverage experimental data to solve the governing equations, we need an estimate of the group velocity. While in principle we could determine this group velocity directly from experimental measurements of the dispersion, $\omega(k_y)$, spatial aliasing from the probe spacing precluded a direct measurement of the wavenumbers of interest. We discussed this aliasing limitation at length in Ref. [18]. Ultimately, in this previous work, we were able to conclude from an analysis of the EDI resonances that the dispersion of the measured oscillations in the test article (Fig. 1) follows the real component of the theoretical EDI dielectric response: [11, 24]:

$$\epsilon^{(1)} = 1 + k^2\lambda_{De}^2 + g(\Omega, X, Y) - \frac{k^2\lambda_{De}^2\omega_{pi}^2}{(\omega - k_x v_p)^2}, \quad (7)$$

where g(Ω, X, Y) is the Gordeev function, $\Omega = (\omega - k_y V_d)/\omega_{ce}$, $X = (k_x^2 + k_y^2)\rho^2$, and $Y = k_z^2\rho^2$. Here V_D denotes the azimuthal electron drift, ω_{ce} is the electron cyclotron frequency, ω_{pi} is the ion plasma frequency,v_p is the axial ion beam velocity, λ_{De} is the Debye length, and $\rho = V_{the}/\omega_{ce}$ is the electron Larmor radius at thermal velocity $V_{the} = \sqrt{T_e/M_e}$ where T_e is expressed in terms of energy. To evaluate Eq. 7, we employed plasma parameters from previous studies of the test article: $n_0 = 8 \times 10^{17} m^{-3}$, $\omega_{ce} = 53$ GHz, $V_D = 526$ km/s, $v_p = 14$ km/s, and $T_e = 15$ eV[26]. Furthermore, we have assumed an axial wavenumber number of $k_x = k_y \sin(15^o)$ based on estimates of the wave propagation angle[18, 27] and a radial wavenumber of $k_z\lambda_{De} = 0.03$, where λ_{De} is the Debye length. This corresponds to a wavelength on the order of the channel width [28–30].

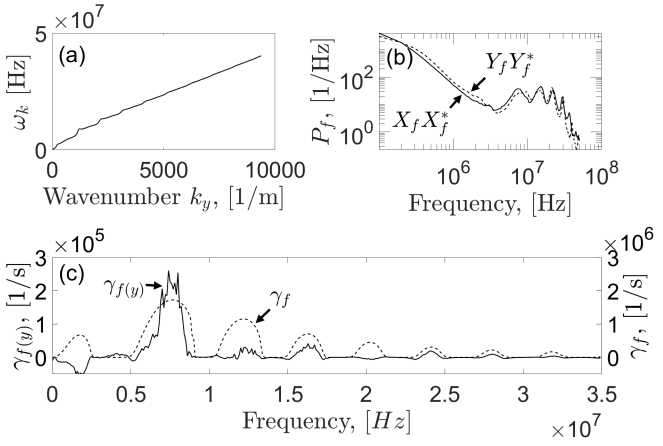

FIG. 2: (a) Dispersion relation of the EDI at the probe location (b) Experimentally measured power spectra for both probe locations. (c) Comparison between the measured azimuthal growth rate $\gamma_{f(y)}$ (left axis) and the growth rate calculated from the dispersion relation γ_f (right axis).

Fig. 2a) shows the dispersion inferred from the solution of Eq. 7 using these experimental measurements of background properties. The result is approximately linear with slight undulations at the cyclotron resonances: $k_y = n\omega_{ce}/V_d$, where n is the harmonic number. At wavenumbers below the first cyclotron resonance ($f < 2$ MHz), the dispersion transitions to the so-called modified two-stream instability (MTSI) [4, 17]. We ultimately used the dispersion shown in Fig. 2a) to infer the group velocity in the azimuthal direction. Furthermore, when used with our experimental data, we convert from a function of wavenumber, $v_g(k)$, to a function of frequency $v_g(\omega)$ through the dispersion relation ($\omega(k)$). We also convert the theoretical growth rate from wavenumber to frequency space, $\gamma_k \rightarrow \gamma_f$, for comparison with the measured growth rate using the same method.

We now turn to experimentally assessing the wave properties of the EDI. For our investigation, we employed the H9, a 9-kW class Hall effect thruster (Fig. 1) with

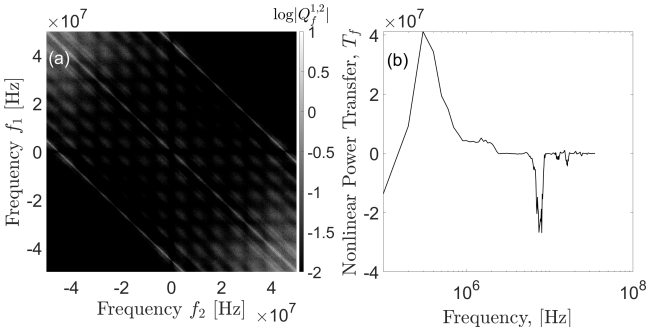

FIG. 3: (a) Nonlinear transfer function $|Q_f^{1,2}|$. (b) Nonlinear power transfer function, T_f.

approximately 30 cm diameter and 15 cm depth. We operated this system at a 300 V 15 A discharge on xenon gas in a 6 m × 9 m vacuum facility. Base pressures during testing, as measured in the plane of the thruster, were 3×10^{-6} Torr-xenon. We used two ion saturation probes with a separation of 1 cm, following the method described in Ref. [18], to estimate oscillations in ion density. For the dispersion relation of the EDI [15] subject to the Hall thruster plasma properties, it can be shown that these density measurements are a proxy for potential oscillations: $\hat{n}_i/n_{i0} \approx \hat{\phi}/T_e$, where $\hat{x}$ is the perturbed density or potential.

We placed the probes 6 mm downstream of the thruster exit plane, which was approximately 1-2 mm downstream of the peak $E \times B$ velocity. The probe signals were sampled at 100 MHz for 2 mega-samples and then subdivided into 2000 realizations for ensemble averaging. As discussed in Ref. [18], this probing method relies on inserting an element into the plasma and thus may perturb the measurement. While we cannot preclude the possibility of probe-induced effects, we found thruster operation remained unchanged with probe insertion, and the features of the EDI spectra persisted in the downstream locations where probe perturbations are expected to be less severe.

Leveraging these experimental methods, we first consider the ensemble averaged power spectra, $\langle X_f X_f^* \rangle$ and $\langle Y_f Y_f^* \rangle$ at each probe location (Figure 2b). Both spectra are characterized by broadband turbulence in the 100 kHz - 2 MHz range with discrete peaks spaced approximately 7 MHz in the high frequency range. We previously showed that these peaks are correlated with cyclotron resonances of the EDI [18]. The close correspondence between the two power spectra also confirms the stationary assumption.

Figure 2c) shows the azimuthal growth rate calculated from the adapted Ritz and Kim algorithm, $\gamma_{f(y)}$, compared to the growth rate predicted from the theoretical dispersion relation, γ_f, determined from Eq. 7. This result is, to the authors' knowledge, the first experimental measurement of EDI growth in this type of crossed-field device. We qualify this result by noting we did not attempt to measure spatial gradients of the spectra in the axial and radial directions—finite values of these may lead to a difference in $\gamma_{f(y)}$ and γ_f. Regardless, we find a number of novel insights from the comparison of theory and measurement. First, there is qualitative agreement in the curve shapes—both trends exhibit peaked growth at several of the same frequencies. This is physically intuitive as these frequencies correspond to the cyclotron resonances where energy is most efficiently extracted from the plasma. Second, unlike the theoretical dispersion, the measured growth exhibits a negative value at the frequencies related to the MTSI ($f \sim 1.5$ MHz). This observation is a departure from previous numerical studies of the MTSI where active damping was not observed, e.g [17]. Physically, our result suggests that the spectrum loses energy to the plasma at this smaller frequency/ longer length-scale. This damping could be attributed to a number of effects such as ion-neutral collisions or spatial gradients in the plasma preventing the propagation of long wavelength (low frequency) EDI/MTSI modes. Third, the magnitudes of the experimentally-measured azimuthal growth rates, $\gamma_{f(y)}$, are an order of magnitude smaller than the values inferred from the theoretical dispersion relation, γ_f.

We consider two limiting cases to interpret this last result. The first scenario is if spatial growth in the axial and radial directions is negligible, $\gamma_f = \gamma_{f(y)}$. This is plausible as the instability's energy source is primarily in the $E \times B$ direction. In this case, our result would suggest there is a mechanism that maintains the shape of the theoretical growth but depresses the magnitude. Previous numerical studies on the EDI, for example, have proposed quasi-linear distortion of the electron distribution function by the waves may lead to such a result [8, 29]. As a second interpretation, we consider the case where there is finite spatial growth in the axial direction but neglect radial growth by symmetry. In this case, it can be shown that $\gamma_f \approx \gamma_{f(y)} + (v_p/2) P_f^{-1} \partial x P_f$—the total growth rate is the combination of the measurement and a contribution dictated by axial convection of wave energy. Assuming the typical gradient length-scales in the axial direction are on the order of 1 mm [18], the convective term could dominate such that $\gamma_f \approx (v_p/2) P_f^{-1} \partial x P_f$. This type of scaling, which is a major departure from linear theory, is consistent with previous numerical investigations where it was suggested that after quasi-linear distortion occurs, wave convection may dictate the growth [8, 29].

We next consider the nonlinear growth by showing in Figure 3a) the magnitude of the nonlinear transfer function ($|Q_f^{1,2}|$). The intensities in this result indicate the degree to which the frequency combination, f_1 and f_2, couples to a third mode at $f_1 \pm f_2$. Negative frequencies in Figure 3a) denote taking the difference between f_1 and f_2. The near-zero amplitudes in the upper right and lower left quadrants generally indicate that there

is no coupling from lower to higher frequency modes: $|f_1| + |f_2| > f_1, f_2$. There is an exception along the line $f_1 + f_2 = 45$ MHz, but we suspect these results are non-physical as the spectral content in this region approached the noise floor. On the other hand, the intensities are largest with clearly defined peaks in the top-left and bottom-right quadrants and close to the -45° axis. The content in these regions indicates strong coupling from high to low order modes $|f_1|, |f_2| > f$. Physically, the combination of trends in Fig. 3a) are indicative of an inverse cascade where energy is nonlinearly coupled from higher to lower frequency modes.

Fig. 3b) illustrates this inverse cascade explicitly by showing the total nonlinear power transfer rate, T_f. The negative peak at the high frequencies commensurate with the cyclotron resonances (f = 5-10 MHz) indicates that some of the energy that is linearly coupled into the waves from the plasma(Fig. 2c) is then transferred away through nonlinear processes. This energy is then deposited at the lower frequency range where the dispersion transitions into the MTSI (f < 2 MHz). This transfer is represented by the positive peak in T_f in this frequency range. The energy then is removed from the spectrum through linear damping (Fig. 2c). This experimental interpretation agrees with recent simulations that suggested the saturation of the EDI involves an initial linear growth of high frequency resonances followed by a nonlinear inverse energy cascade[4, 17, 28]. Although, we note that comparisons to simulation are only appropriate for the final stationary state of the oscillations: our method only resolves the saturated state and cannot detect the different stages of evolution explored in Ref[17] before the instability reaches saturation.

In summary, we have performed the first direct experimental measurements of the nonlinear and linear growth of the EDI in a Hall effect discharge. We have shown that while the measured linear growth confirms the EDI is driven unstable by cyclotron resonances, there are notable departures from simple linearized theory. We also have found experimental evidence that a nonlinear energy cascade to lower frequencies and larger length-scales exists. Both of these experimental insights have direct implications for understanding the application-driven question of how this instability interacts with the fundamental plasma state. Indeed, in order to approximate "anomalous" wave-driven transport, we must know both the effective growth rate and shape/magnitude of the power spectra [14]. As numerical simulations and experimental results have previously suggested, however, simple linear theory based on assuming a thermalized distribution is not sufficient to capture the actual growth rate[26]. Our experimental findings confirm this conclusion.

With this in mind, the measurement of the growth rate as a function of position in the plasma could lead to simplified models of cross-field transport that would enable predictive modelling of crossed-field devices. To this point, one interpretation of our experimental results is that the growth rate may simply depend on wave convection. As was previously discussed in Ref. [29], this assumption may be leveraged to identify simple closure models. Finally, we remark that in order to make our measurements, we have used a technique adapted from previously derived bispectral analysis that is more conducive for use in low temperature plasmas with smaller devices. This same methodology, in principle, can be extended to a wide range of systems beyond the EDI to answer outstanding questions about the physics of transport-inducing instabilities.

This work was supported by an AFOSR Young Investigator Award through the Space Propulsion and Power program. The authors also would like to thank P. Roberts and T. Marks of the University of Michigan for helpful discussions and edits.

* brownzac@umich.edu

[1] S. P. Gary, Journal of Geophysical Research: Space Physics **86**, 4331 (1981).
[2] O. Koshkarov, A. Smolyakov, Y. Raitses, and I. Kaganovich, Phys. Rev. Lett. **122**, 185001 (2019).
[3] M. Keidar and I. Beilis, IEEE Transactions on Plasma Science **34**, 804 (2006).
[4] S. Janhunen, A. Smolyakov, O. Chapurin, D. Sydorenko, I. Kaganovich, and Y. Raitses, Physics of Plasmas **25**, 011608 (2018).
[5] I. D. Kaganovich, A. Smolyakov, Y. Raitses, E. Ahedo, I. G. Mikellides, B. Jorns, F. Taccogna, R. Gueroult, S. Tsikata, A. Bourdon, J.-P. Boeuf, M. Keidar, A. T. Powis, M. Merino, M. Cappelli, K. Hara, J. A. Carlsson, N. J. Fisch, P. Chabert, I. Schweigert, T. Lafleur, K. Matyash, A. V. Khrabrov, R. W. Boswell, and A. Fruchtman, Physics of Plasmas **27**, 120601 (2020), https://doi.org/10.1063/5.0010135.
[6] S. Tsikata and T. Minea, Physics Review Letters **114**, 185001 (2015).
[7] M. E. Koepke, Reviews of Geophysics **46** (2008).
[8] T. Lafleur, S. D. Baalrud, and P. Chabert, Physics of Plasmas **23**, 053502 (2016).
[9] J. P. Boeuf and L. Garrigues, Physics of Plasmas **25**, 061204 (2018).
[10] S. P. Gary and J. J. Sanderson, Journal of Plasma Physics **4**, 739 (1970).
[11] D. Forslund, R. Morse, C. Nielson, and J. Fu, The Physics of Fluids **15**, 1303 (1972), https://aip.scitation.org/doi/pdf/10.1063/1.1694082.
[12] M. Haines, Nuclear Fusion **17**, 811 (1977).
[13] L. B. Wilson III, C. A. Cattell, P. J. Kellogg, K. Goetz, K. Kersten, J. C. Kasper, A. Szabo, and M. Wilber, Journal of Geophysical Research: Space Physics **115** (2010).
[14] R. Davidson and N. Krall, Nuclear Fusion **17**, 1313 (1977).
[15] A. Ducrocq, J. C. Adam, and A. Heron, Physics of Plasmas **13** (2006).
[16] T. Lafleur, P. Chabert, and A. Bourdon, Physics of Plas-

mas **25**, 061202 (2018).
[17] S. Janhunen, A. Sydorenko, D. Sydorenko, M. Jimenez, I. Kaganovich, and Y. Raitses, Physics of Plasmas **25**, 082308 (2018).
[18] Z. A. Brown and B. A. Jorns, Physics of Plasmas **26**, 113504 (2019).
[19] A. Tavassoli, A. Smolyakov, M. Shoucri, and R. J. Spiteri, Physics of Plasmas **29**, 030701 (2022), https://doi.org/10.1063/5.0083081.
[20] C. P. Ritz, E. J. Powers, and R. Bengtson, Physics of Fluids B: Plasma Physics **1** (1989).
[21] J. S. Kim, R. Durst, R. Fonck, E. Fernandez, A. Ware, and P. W. Terry, Physics of Plasmas **3**, 3998 (1996).
[22] R. Z. Sagdeev and A. A. Galeev, *Nonlinear Plasma Theory* (New York: Benjamin, 1969).
[23] Z. A. Brown, *Small-scale Instability Driven Electron Transport in Hall Thrusters*, Ph.D. thesis, University of Michigan (2022-In Preparation).
[24] J. Cavalier, G. Lemonie, N amd Bonhomme, S. Tsikata, C. Honore, and D. Gresillon, Physics of Plasmas **20**, 082108 (2013).
[25] C. Ritz and E. Powers, Physica D: Nonlinear Phenomena **20**, 320 (1986).
[26] Z. Brown and B. Jorns, in *AIAA Propulsion and Energy 2021 Forum* (2021) https://arc.aiaa.org/doi/pdf/10.2514/6.2021-3415.
[27] S. Tsikata, N. Lemoine, V. Pisarev, and D. M. Gresillon, Physics of Plasmas **16**, 033506 (2009).
[28] M. Sengupta and A. Smolyakov, Physics of Plasmas **27**, 022309 (2020).
[29] T. Lafleur, S. D. Baalrud, and P. Chabert, Physics of Plasmas **23**, 053503 (2016).
[30] F. Taccogna, P. Minelli, Z. Asadi, and G. Bogopolsky, Plasma Sources Science and Technology **28**, 064002 (2019).